Contract No.:

This manuscript has been authored by Battelle Savannah River Alliance (BSRA), LLC under Contract No. 89303321CEM000080 with the U.S. Department of Energy (DOE) Office of Environmental Management (EM).

NOVEL NANOPHOTOCATALYSTS FOR DETECTION AND REMEDIATION OF CONTAMINATED ECOSYSTEMS

Simona E. Hunyadi Murph*[1,2] and Patrick Gaulden[1]

[1]Savannah River National Laboratory
Environmental and Legacy Management Directorate
Aiken, South Carolina, USA

[2] University of Georgia
Department of Physics and Astronomy
Athens, Georgia, USA

*Corresponding author, E-Mail address: Simona.Murph@srnl.doe.gov, Phone: 803-646-6761

Abstract

Monitoring the level of contaminants in aquatic environment is critical for the protection of both human health and ecosystem function. Remediation and management of contaminated sites is often technically difficult and costly when there are large volumes of contaminated material. We developed a novel in situ detection and remediation capability able to acquire, display and disseminate real time pollution data. Specifically, we designed and created metal matrix hybrid composite comprised of: (a) iron oxide (Fe_2O_3),, (b) iron oxide-silica (Fe_2O_3/SiO_2), (c) iron oxide-silica-titania ($Fe_2O_3/SiO_2/TiO_2$), and (d) iron oxide-silica-titania-gold ($Fe_2O_3/SiO_2/TiO_2/Au$) nanoparticles that are effective, environmentally friendly and can be readily deployed at various contaminated sites for monitoring of water polluted organic contaminants.

Keywords: nanomaterials, environmental stewardship, organic contaminants, photodegradation.

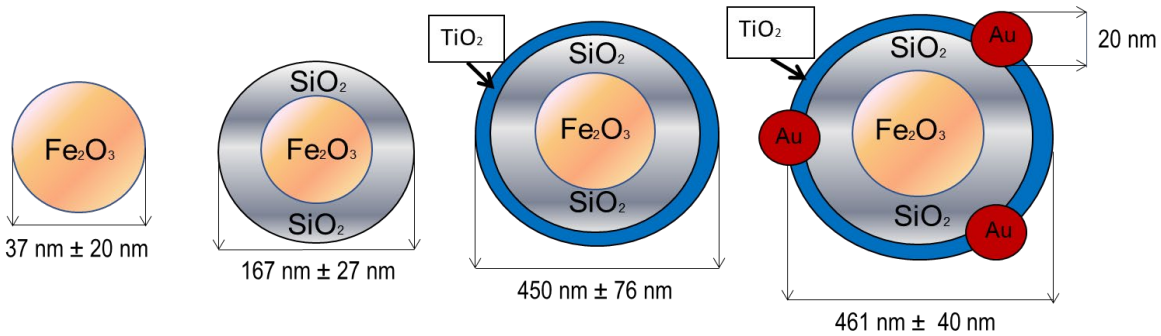

(a) (b) (c) (d)

1. Introduction

A clean ecosystem is essential to life. The world is facing formidable challenges in meeting ever increasing demands in reducing environmental contamination [1, 2]. Persistent organic pollutants [3], heavy metals [4], and radionuclides [5] all contribute to environmental problems threatening both humans and ecosystem biota. Trace detection and treatment of these pollutants challenges us to constantly improve our monitoring and remediation technology [6, 7]. The large-scale cleanup of contaminated sites requires innovations in engineering and understanding of the fundamental chemistry of both the monitoring and remediation process to advance these technologies.

The development of efficient and sustainable technologies for remediation of contaminated ecosystems has been the focus of many studies [1-5]. For example, degradation of contaminants can be achieved with the help of nanomaterials [1]. Nanotechnology provides a powerful avenue for detection and treatment of trace pollutants in the environment [8]. Nanomaterials have a number of key physicochemical properties that make them particularly attractive as separation media for contaminant measurement and water purification [1, 3, 4]. For example, (i) on a mass basis, they have much larger surface areas than bulk particles [1]; (ii) nanomaterials can also be functionalized with various chemical groups to increase their affinity toward a given compound [6]; (iii) they can also serve as high capacity, selective, recyclable supports, and ligands for toxic organics, metal ions, and radionuclides [1-5]; (iv) metallic nanoparticles also demonstrate exciting properties [1, 7, 9, 10, 11, 12] which offer capabilities such as single molecule detection [1, 4]; optical imaging [1], photothermal [10] and magnetothermal therapies [11]; and (v) hybrid nanostructures combine physicochemical properties of two or more nanomaterials opening the door to a wider landscape of applications. For example, magneto-optically responsive nanostructures were used as positive contrast agents for magnetic resonance imaging [12], magneto-thermal release of isotopes [11, 13], effective removal of radionuclides [14], and sensing applications [1, 4, 6].

Titanium dioxide (TiO_2 or titania), an inexpensive and abundant material, has been known to be an exceptional photocatalyst for many reactions, including water splitting, degradation of organic pollutants and synthetic fuel production [1, 3, 15, 16]. . The optical to chemical conversion efficiency, however, has generally been very low. This is because titania has a very narrow band edge absorbance and provide limited amounts of free electrons and protons on the surface for such processes. The efficiency of titania for photocatalytic applications is severely limited by its large band gap (~3.2 eV). As a result, titania can use less than approximately 5% of the solar spectrum (ultraviolet region) [3].

Several approaches have been taken to extend the wavelength range that absorb light at lower photon energies, thus extending absorption into the visible light region of the spectrum. Methods include doping with non-metals and/or metals [17], or combining titania with lower band gap semiconductors to create junctions that decreases electron-hole pair recombination [18]. One of the most well-studied materials for extending titania's visible light photocatalytic properties is gold [3]. In its bulk state, gold is relatively inert, but at the nanoscale gold has remarkable unique properties. At the nanoscale, gold nanoparticles show localized surface plasmon resonance (LSPR) in which the free electrons collectively oscillate when resonantly driven by electromagnetic radiation [1, 10]. The strong absorbance and scattering generated in gold nanoparticles generate

intense and highly confined electromagnetic fields that are determined and tailored by the nanoparticle's size, geometry and environment. In hybrid nanomaterials, such as gold-titania, gold nanoparticles can absorb visible light due to localized surface plasmon resonance and then inject the excited electrons into the conduction band of titania or can also act as electron reservoirs, further increasing photocatalytic activity in the ultraviolet and visible range [3].

Iron (III) oxide (Fe_2O_3 or maghemite) [11, 13, 19, 20], is a well-studied semiconductor and abundant photocatalyst. The band gap of iron oxide nanoparticles is 2.2 eV, allowing the possibility of enhanced charge separation. Iron oxide has received a great deal of attention because of its magnetic properties which allow it to be retrieved from the environment. This minimizes the ecological footprint and creates a more economical catalyst through easy manipulation and recycling.

Coupling of iron oxide with other nanomaterials with distinctive properties have been explored in the scientific community. This is due to the interest in creating hybrid nanostructures with enhanced physico-chemical properties. The augmented properties of the composite nanomaterials, in comparison with individual component materials, have been exploited in catalysis, medical, environmental, sensing, imaging fields, among others [1, 4, 7, 10, 11, 12]. For example, we reported earlier that the combination of gold nanoparticles with iron (III) oxide was more efficient in plasmonic heating applications than pure gold nanoparticles, making the hybrid material an economically viable material [10, 20]. Energy, in the form of an induced alternating magnetic field, can be also selectively coupled to hybrid magnetic-hydride iron-oxide-palladium nanomaterials for the selective and controlled release of hydrogen gas isotopes [11]. Multifunctional iron oxide-gold composite nanostructures with tailored nano-gap junctions have been produced via a multi-seed-mediated approach and investigated for analyte detection [7].

This research describes a facile sol-gel method [6] for creating hybrid iron (III) oxide-titania nanomaterials decorated with gold nanoparticles for environmental remediation applications. The multifunctional composite nanomaterials allow for photocatalyzed reactions to occur in both visible and ultraviolet regime. The photocatalytic activity of the synthesized hybrid nanoparticles for breaking down a model analyte, methyl orange (MO), was explored. The efficiency of the photocatalyst under ultraviolet light irradiation was measured and compared to titanium oxide and iron oxide nanoparticles.

2. Materials and Instrumentation

Chloroauric acid trihydrate ($HAuCl_4$), trisodium citrate (>99%), iron (III) oxide nanopowder (<50 nm), tetraorthosilicate, ethanol, aqueous ammonia (5N solution), High purity methyl orange (MO, chemical formula, $C_{14}H_{14}N_3NaO_3S$), and titanium (IV) tert-butoxide were purchased from Sigma Aldrich. All materials were used as received. All glassware used in the following protocols was cleaned with Aqua Regia and then rinsed with deionized water. All aqueous solutions were prepared in deionized water. A *Fischer Scientific* accuSpin Micro17R was used for centrifuging the gold nanoparticles. A *TECS USA* MCS PDA with LS ultraviolet–visible was used to evaluate nanoparticle's optical properties and the rate of degradation for methyl orange. The Zeta sizer and Zeta potential of the nanoparticles were obtained using a *Brookhaven Instruments* DLS NanoBrook Omni (110-240 V) manufactured in 2014. A *Hitachi* SU8200 Scanning Electron

Microscope coupled with energy dispersive X-Ray spectroscopy was used for evaluating nanomaterials morphologies and compositions.

3. Experimental Section

3.1 Iron oxide/silica nanoparticles synthesis

Fabrication of the iron oxide/silica nanoparticles followed a modified version of a previously reported sol-gel method [6, 22]. A stock solution of iron oxide nanoparticles was prepared using 0.04 g of iron oxide (III) nanopowder (MW = 159.69 g mol-1) with 10 mL deionized water as solvent. 3 mL deionized water was added to the tube using a pipette, followed by addition of 100 µL of iron oxide nanoparticle solution. The solution was then sonicated for even dispersion. Then 5 mL of 3.4 mM sodium citrate solution (0.05 g in 50 mL water) was added. The solution was stirred for 1 hour, and the nanoparticles were collected using a magnet. Nanoparticles were subsequently dispersed into 4mL of ethanol and 2 mL of 5 N aqueous ammonia. After 30 min stirring process, 100 µL of tetraethyl orthosilicate (TEOS, MW = 208.33 g mol−1) was added. Stirring continued for 4 hours. Sample was sonicated for 15 minutes. The sample was separated from the supernatant by a magnet and washed several times before being dispersed in water. These particles were characterized by ultraviolet-Vis, Zeta potential/DLS, and scanning electron microscopy analysis before adding the additional titania layer and gold nanoparticles.

3.2 Core-shell hybrid (iron oxide/silica)/titania gold decorated nanostructures preparation

The iron oxide/silica particles were extracted and dispersed in 2 mL of absolute ethanol and 10 µL of water. 2, 5, 10, and 20 µL injections of titanium (IV) tert-butoxide (TTB, 97%) were added under argon atmosphere in 2 mL of ethanol solution. The tert-butoxide ethanolic solution was then added to the/silica solution to directly coat a layer of titania onto the surface of the iron oxide/silica particles. Mixing continued for about 16 h. Afterward the particles were washed in absolute ethanol, then ethanol and water (1:1), and then pure water. The iron oxide/silica/titania particles were separated from the supernatant using a magnet. Decoration of gold nanoparticles was performed following a previously defined sol-gel method by our group [3], resulting in the desired, novel nanomaterials for use in photocatalytic degradation experiments. Iron oxide/silica/titania particles were placed 3 mL of 1% trisodium citrate solution and stirred for 10 minutes. Then the solution was added to a 25 mL flask containing 7 mL of water. The solution was heated to 100 ºC and stirred using a glass stir rod. Once the solution began to boil, 100 µL of 0.01 M chloroauric acid solution was added and stirring continued for 8 minutes. The solution changed from a brown color to a red-pink colored solution. The flask was then removed from heat and allowed to cool to room temperature. The gold decorated iron oxide/silica/titania nanoparticles were then separated and collected using a magnet. The particles were then characterized and tested for photocatalytic efficiency. After cooling, the iron oxide/silica/titania/gold solution was placed in a conical tube and placed directly above a neodymium magnet for 30 minutes. The particles were allowed to re-disperse into the washing solution and were collected again using the magnet. This re-dispersion was repeated several times to remove the supernatant and/or unattached nanoparticles. The

nanoparticles were extracted from the bottom of the conical tube using a micropipette for further analysis.

3.3 Monitoring photocatalytic and photodegradation activity

The photocatalytic activity of the synthesized iron oxide/silica/titania/gold nanoparticles was investigated by the photodegradation of a model analyte, methyl orange (MO, 0.05 mM) dye, in water. The nanoparticles were extracted from solution (0.5 mL of particle solution, starting with 100 µL of stock solution in 5 mL of water) and placed in 1 mL of dye solution inside a plastic cuvette. A blank standard was also prepared for comparison of photodegradation without the presence of nanophotocatalysts. The solution was then irradiated by a 400 W mercury lamp and/or an ultraviolet lamp (135 mW/cm^2, 365 nm). The absorbance of the sample at 464 nm was measured over time in 1-hour increments to measure the relative drop in concentration of the model analyte. The results of these measurements were compared to the photocatalytic activity of "as-purchased" iron oxide nanoparticles as a standard, as well as titania nanoparticles, for comparison.

4. Results and Discussion

4.1 Synthesis and characterization of gold decorated iron oxide/silica/titania nanoparticles

Iron oxide nanoparticles were placed in deionized water and sonicated prior to characterization and decoration. The reported size distribution (determined by BET surface area measurement reported by Sigma-Aldrich) states that the size of the particles is less than 50 nm. This was confirmed by scanning electron microscopy analysis conducted by us. The nanoparticle's size distribution, however, ranged from around 10-200 nm (Figure 1a).

Coating of the iron oxide nanoparticles with a layer of silica and titania after citrate surface functionalization was accomplished through a sol-gel approach. The sol-gel reaction occurs through a series of steps including hydrolysis and condensation [6, 21, 22]. In this reaction, tetraethyl orthosilicate in ethanol media was used as a precursor to create the gel-like shell structure in the presence of a basic catalyst, i. e. ammonia. Silica shell (SiO_2) was created on the iron oxide nanoparticle's surface as these iron oxide nanoparticle structures serve as nucleation centers for shell deposition. While silica is not catalytically active in the ultraviolet-visible range, it acts as a stable foundation for titania, increasing its lifetime stability and efficiency [23]. For example, our previous studies showed that core-shell silica-titania display four times improvement in the photocatalytic response than titania nanoarrays [3]. This was attributed to the creation of individual nanocrystals titania in silica, leading to an increase in surface area and/or higher porosity of the silica surface.

In Figure 1 b, the iron oxide/silica nanoparticles produced are shown to have a size distribution of 158 nm ± 27 nm. This demonstrates successful creation of core-shell hybrid nanomaterials. The increase in particle diameter from the original approximatively 50 nm is significant. While not explored in this study, small modification in the precursors concentration and reaction temperature can be used to control the silica shell thickness [6, 21, 22]. Interestingly, scanning electron microscopy images shows that the core-shell nanostructures are aggregates comprised of multiple iron oxide nanoparticles coated by a silica shell. The shell size was relatively uniform, with an average of 35 nm ± 10 nm thickness. The statistical size distribution and respective surface charge of the nanoparticles is shown in Table 1. The particles also had significant agglomeration, which was able to be corrected by surfactant addition (sodium citrate) and sonication. This is not surprising as the iron oxide nanoparticles are ferromagnetic [11]. After silica formation, the effective surface charge of the nanoparticles changed from -10 mV to -45 mV (Table 1), which corresponds to the high negative charge of deprotonated silanol groups in the silica shell at the pH values of 6-7. The original -10mV surface charge value of iron oxide is due to hydroxide ions adsorbed on the surface, specifically the deprotonated −Fe−OH species present on the nanoparticle's surface [10, 11].

To prepare a shell of ultraviolet-active titania shell, the iron oxide/silica nanoparticles were placed in an ethanolic solution. Small aliquots of water were also added to the reaction. Titania precursor, titanium tert-butoxide (TTB), in absolute ethanol (to prevent hydrolysis in air), was subsequently added to the iron oxide/silica nanoparticle nanoparticle's solution. This process allows a slow condensation of tert-butoxide. The condensation occurred around the silica shell of the iron oxide. Different aliquots of tert-butoxide were added as a way to tailoring the shell thickness (Table 1). The scanning electron images presented in Figure 1(c) are representative of the iron oxide/silica/titania sample containing the largest amount of tert-butoxide (20 µL tert-butoxide added in ethanol). The size distribution of the sample was approximately 450 nm ± 76 nm. The zeta potential changed to -9 mV after titania shell deposition from -45 mV. This demonstrates successful titania deposition. The scanning electron microscopy images were collected on the nanocomposite sample (Figure 1c). The energy dispersive X-ray analysis confirms the presence of specific elements (data not shown).

Table 1. Size distribution and surface charge of nanoparticles.

	Iron oxide	**Iron oxide/Silica**	**Iron oxide/Silica/Titania**
Diameter (nm)	37 ± 20	167 ± 27	450 ± 76
ζ-potential (mV)	-10	-45	-9

Gold nanospheres were decorated onto the surface of the core-shell hybrid iron oxide-silica-titania nanomaterials by using a citrate reduction method [1, 7, 10]. In this procedure, the core-shell nanostructures serve as support to grow gold nanospheres [10, 12, 20]. The distribution of gold throughout the sample appeared to be uniform and the size of the gold nanospheres ranged from 15-22 nm (Figure 1(d)). The backscattering electron (BSE) detector was used to further

discriminate between electron dense (gold) and non-electron dense (silica/titania) particulates. Gold nanospheres were easily observed – dark spots (Figure 1f).

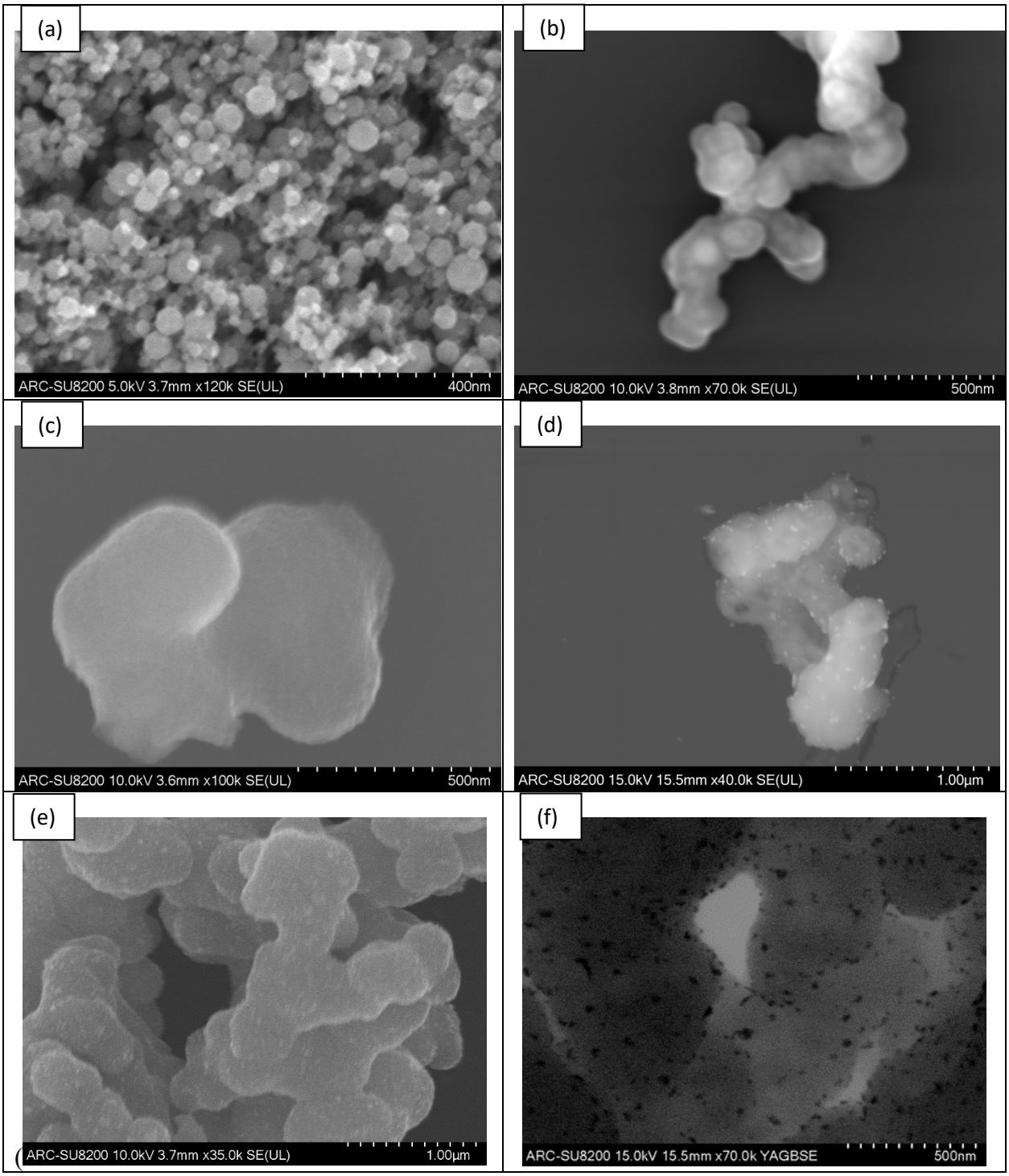

Figure 1. Scanning electron microscopy images of nanoparticles; (a) iron oxide nanoparticles (<50 nm); (b) iron oxide/silica nanoparticles; (c) iron oxide/ silica/titania nanoparticles; (d, e, f) Gold decorated iron oxide/silica/titania nanoparticles.

By controlling the concentration of the titania precursor, the thickness of the shell can be tailored to the desired dimensions. In this case, different variations of the tert-butoxide concentration leads to differences in nanoparticle's sizes. As expected, an increased in concenration leads to larger size particles from 75 nm to 150 nm (Figure 2).

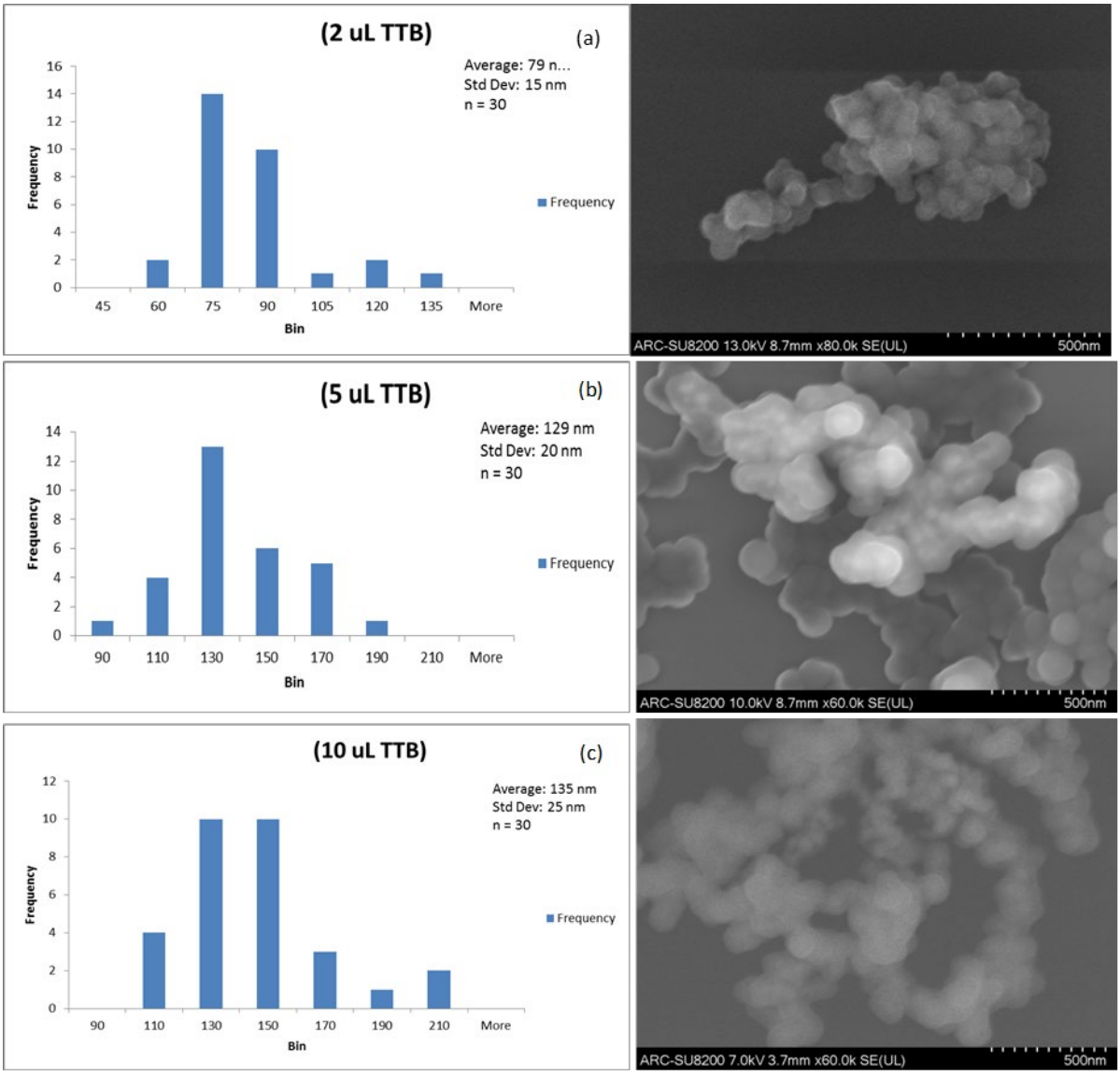

Figure 2. Scanning electron microscopy images and size distribution histograms for three samples of iron oxide/silica/titania nanoparticles with different amounts of titanium tert-butoxide precursor, (a) 2 uL; (b) 5 uL; (c) 10 uL.

In addition to size change and surface charge analysis, elemental composition of each sample was monitored and confirmed using energy dispersive spectroscopy, EDS., Spectra collected from the iron oxide/silica/titania sample are shown in Figure 3. The weight percentages of each element are also shown, with titanium having the highest percent weight of the metals. The collection of spectra was accompanied by energy dispersive spectroscopy mapping to identify areas of specific elemental concentration.

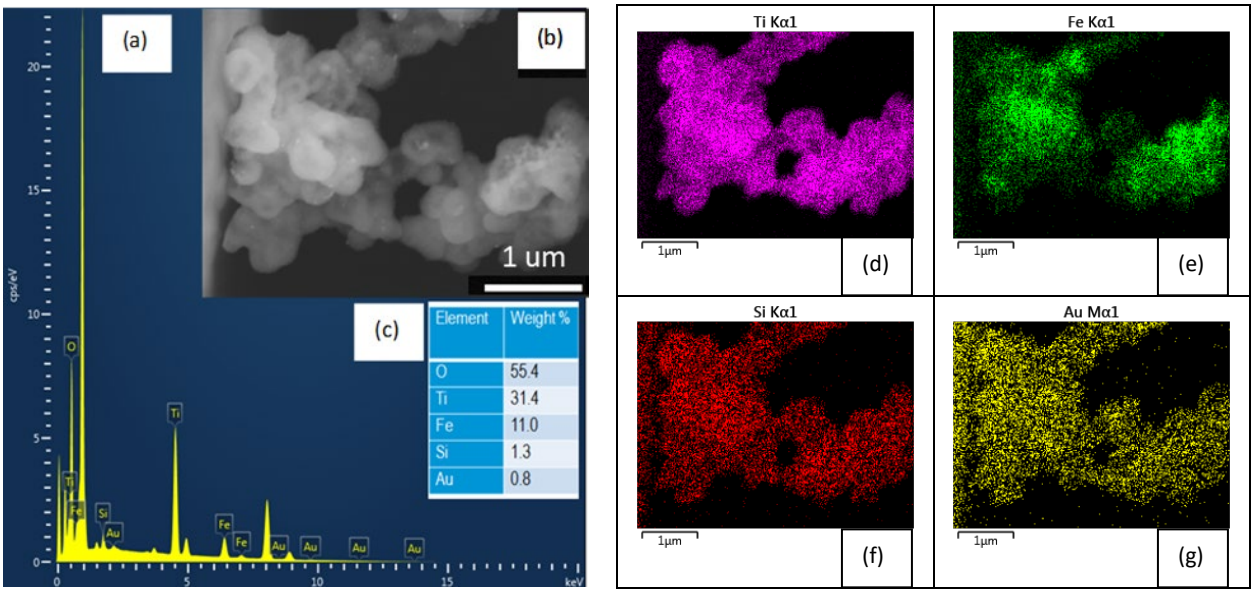

Figure 3. (a) Energy dispersive spectroscopy spectrum and mapping of iron oxide/silica/titania nanophotocatalyst; (b) Scanning electron microscopy image inset; (c) elemental percent weight composition table; (d) titanium map; (e) iron map; (f) silicon map; (g) gold map.

4.3. Photocatalytic degradation of organic contaminant

Titania is a benchmark material for catalytic processes due to its favorable properties, such as powerful oxidation capability, superior charge transport, and corrosion resistance [3]. Titania is also inexpensive and can be easily produced. Titania-based nanophotocatalysts of various compositions and architectures have been investigated for destruction of organic contaminants, water splitting and conversion of carbon dioxide to fuel [3, 12, 24, 25, 26, 27].

In this study, the photocatalytic activity of the prepared nanophotocatalysts was methodically explored by monitoring changes in the absorbance spectrum of methyl orange. The decrease in peak absorbance at 464 nm (Figure 4 and Figure 5b) was recorded in hourly increments for maximum five hours. The photodegradation experiment was performed in the presence of nano-photocatalysts, at ambient temperature and under UV illumination. The synthesized nanoparticles with the largest titania shell thickness were tested under ultraviolet illumination as titania is active in this regime.

A solution of methyl orange exposed without catalysts was used as a control to evaluate methyl orange's behavior. A small decrease in absorbance for the control solution of methyl orange was recorded within the first hour of ultraviolet light exposure. However, this reduction it stabilized within an hour exposure and can be attributed to self-photosensitization of methyl orange [25]. No additional degradation was recorded in the control experiment even after prolonged exposure for five hours under ultraviolet illumination. It is believed that this is due to the natural breakdown of dyes under ultraviolet irradiation and equilibration process. Iron oxide nanoparticles did not influence the photocatalytic breakdown of methyl orange under ultraviolet light. However, the 25 nm titania nanoparticles were successful in reducing the methyl orange absorption peak by 83% in one hour and nearly 100% after two hours. Nonetheless, when the newly prepared nanophotocatalysts, i. e. iron oxide/silica/titania/gold were tested, the reduction of the 464 nm peak was 84% after five hours. These results are expected as titania is responsive in the ultraviolet region of the spectrum. Within an hour of exposure, the rate of reaction of methyl orange photodegradation is significantly higher when titania nanocatalyst (84%) is used in comparison to iron oxide/silica/titania/gold nanomaterials (42%). However, over time, specifically after five hours of testing, a similar response was achieved (approximately 84% degradation) with iron oxide/silica/titania/gold nanomaterials.

Numerous studies have shown that the titania nanophotocatalyst's size, crystallinity, number/type of defects, electron–hole recombination, and surface area, are important parameters affecting the rate of photocatalytic reactions. Catalyst's surface area is of particular important in catalytic reaction. For example, a larger surface area results in an increased catalytic process due to the larger area of adsorption of reactant and the intermediate species to the catalysts' surface. Increasing the number of active sites also hinders the recombination of charge carriers, electrons and holes, making the catalytic process more efficient [3]. In our studies, there is a significant difference in size between titania nanospheres and iron oxide/silica/titania/gold hybrid nano-photocatalyst. For example, titania nanospheres have a diameter of 25 nm while the hybrid nanostructures are approximately 460 nm in size.

While titania nanospheres are faster nano-catalysts for degradation of methyl orange compared with the hybrid nanomaterials, an advantage of using the nanocomposite materials iron oxide/silica/titania/gold is that they exhibit magnetic properties. These unique property induces external and non-contact manipulation of the material using magnetic fields, i. e. external magnet. This is central to many industrial and environmental processes as often catalysts must be collected and recycled. This is not possible when using titania nanoparticles. The ability to collect and manipulate catalysts with an external magnet is significant when released and used in natural ecosystems. For example, magnetic photocatalysts can be simply reused and recycled after reaction is completed. Additionally, the magnetic collection could eliminate potential unforeseen consequences of releasing unbounded nanomaterials in the environment.

Photographs illustrating magnetic property and manipulation of the hybrid nanomaterials are shown in Figure 5 a. By simply placing a cuvette containing the nanocomposite hybrid nanoparticle solution in a static magnetic field, all of the magnetic nanoparticles are collected within less than 1 minute. This outcome demonstrate that the resulting hybrid nanomaterials retain the properties of the individual magnetic iron oxide original component even after multiple surface modifications with silica, titania and gold nanostructures. This is beneficial as the hybrid structures can be further explored for multiple applications that employs the plasmonic properties of gold

nanoparticles, magnetic properties of iron oxide and photocatalytic activity of titania, such as optical sensing and imaging, hyperthermia applications, magnetic resonance imaging, and catalytic processes.

The photodegradation of methyl orange is based on an advanced oxidation process where hydroxyl radicals are produced. Once generated, these radicals participate in reactions and non-selectively break down organic compounds [24]. The mechanism by which the photodegradation process take place, however, differs under ultraviolet and/or visible light [25]. This is due the fact that components of the photocatalyst material are being triggered by different illumination wavelength leading to different mechanism. Under ultraviolet light, the production of radicals is initiated by direct transitions of electrons in titania from its valence band to its conduction band. Under visible light irradiation, the electrons of the visible light absorbing components (in this case, iron oxide and gold) are transferred to the defect conduction band states of titania. This results in radical formation under both ultraviolet and visible light.

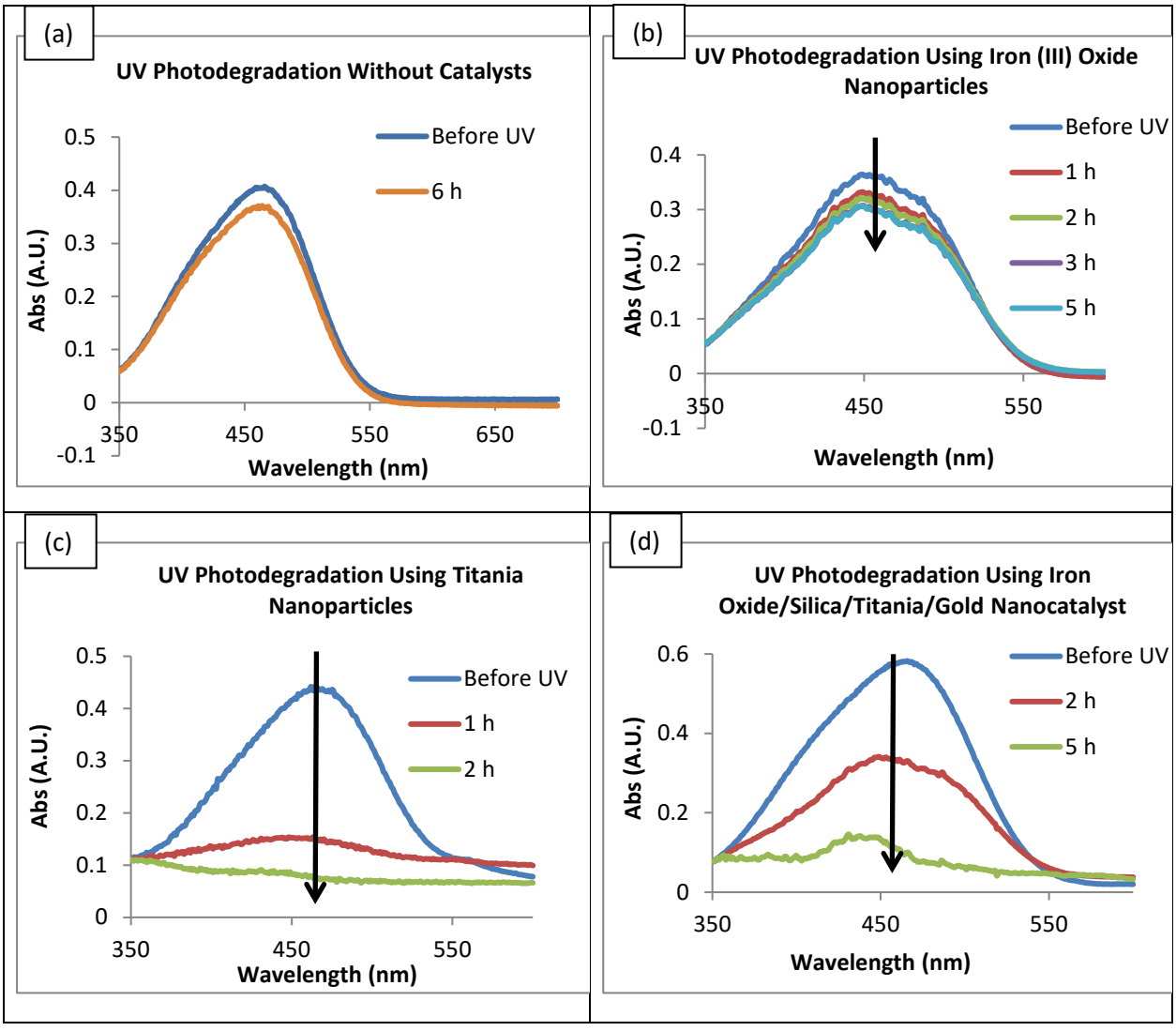

Figure 4. Ultraviolet-Visible absorbance spectra of methyl orange under ultraviolet illumination; (a) without catalysts; (b) with iron oxide nanoparticles; (c) with titania nanoparticles; (d) with iron oxide/silica/titania/gold nanophotocatalysts.

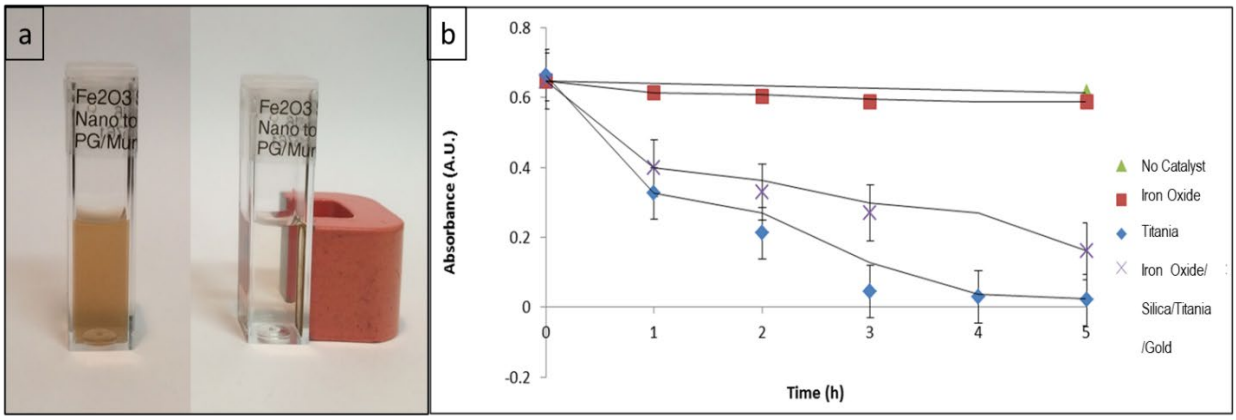

Figure 5. (a) Photographs illustrating magnetic manipulation of the iron oxide/silica/titania/gold in solution (left) before magnetic exposure and (right) an external magnet placed near a cuvette attracts hybrid nanoparticles collecting within <1 minute; (b) Reduction of methyl orange peak absorbance at 464 nm under ultraviolet illumination over 5 hours using different nanophotocatalysts.

5. Conclusions

This study shows the successful preparation, characterization, and evaluation of a novel photocatalytic material that is active in both the ultraviolet and visible region of the spectrum. A facile sol-gel method to creating iron oxide/silica core-shell nanomaterials was employed. A similar process was used to produce an additional titania shell with varying thickness by condensation of different amounts of tert-butoxide at the surface of the iron oxide/silica nanoparticles. Finally, the monodispersed, stable iron oxide/silica/titania nanoparticles were decorated with 20 nm gold spheres by citrate reduction. The iron oxide/silica/titania/gold hybrid nanomaterials retain the properties of the individual magnetic iron oxide original component even after multiple surface modifications. This is beneficial as the hybrid structures can be further explored for multiple applications that employs the plasmonic properties of gold nanoparticles, magnetic properties of iron oxide and photocatalytic activity of titania, such as optical sensing and imaging, hyperthermia applications, magnetic resonance imaging, and catalytic processes.

The photocatalytic activity of the synthesized hybrid nanoparticles for degradation of a model analyte, methyl orange (MO), was monitored using ultraviolet-visible spectroscopy. The composite nanomaterials were then compared to other nano-photocatalysts. The photocatalytic activity of the novel hybrid nanomaterials resulted in an 84% photodegradation after 5 hours of ultraviolet light exposure. These results shows that the hybrid materials could be employed to destroy organic pollutants present in wastewater streams. The magnetic properties of the hybrid nanomaterials will allow easy retrieval, reuse, and recycling. Further testing is underway to

evaluate the effects of titania shell thickness, crystallinity, morphology, and additional wavelength of energy on photocatalytic activity.

6. Acknowledgements

This work was supported by the Laboratory Directed Research and Development (LDRD) program within the Savannah River National Laboratory (SRNL). We would like to thank the Science Undergraduate Laboratory Internship (SULI) operated by the DOE-Office of Science and the Savannah River National Laboratory for financial support. This work was produced by Battelle Savannah River Alliance, LLC under Contract No. 89303321CEM000080 with the U.S. Department of Energy. Publisher acknowledges the U.S. Government license to provide public access under the DOE Public Access Plan (http://energy.gov/downloads/doe-public-access-plan).

7. References

1. Hunyadi Murph S.E., Larsen G., Coopersmith K. (2017) Anisotropic and shape-selective nanomaterials: structure-property relationships, nanostructure science and technology series. Springer Publisher, pp 1- 470.

2. Meidan Ye, (2014) in Low-cost Nanomaterials: Toward Greener and More Efficient Energy Applications, edited by Zhiqun Lin, Jun, pp. 9-17.

3. Hunyadi Murph SE (2020) Shape-Selective Mesoscale Nanoarchitectures: Preparation and Photocatalytic Performance, **Catalysts**, 10:532-552.

4. Srivatsan, T.S., Harrigan W., Hunyadi Murph, S.E. (2021) Metal-Matrix Composites: Advances in Analysis, Measurement, and Observations, Springer Publisher, 1-275.

5. Hunyadi Murph SE, Larsen GK, Korinko P, Coopersmith KJ, Summer AJ, Lewis R. (2017) Nanoparticle Treated Stainless Steel Filters for Metal Vapor Sequestration. **JOM**, 69:162–172.

6. Hunyadi Murph SE, Murphy CJ (2013) Patchy Silica-Coated Silver Nanowires as SERS Substrates. **J. Nanoparticle Res**. 15:1607.

7. Hunyadi Murph SE, Searles, E (2020) Iron Oxide-Gold Composite Nanoparticles and Nano-Gap Junctions for Sensing Applications Using Surface -Enhanced Raman Scattering, in T.S. Srivatsan, W. Harrigan, Hunyadi Murph, S.E. (2021) Metal-Matrix Composites: Advances in Analysis, Measurement, and Observations, Springer Publisher, pp. 93-110.

8. Gautam RK, Chandra M, in Nanomaterials for Wastewater Remediation, edited by Peter Jardim (Cambridge, MA, 2016), pp. 2-18.

9. Tao, CG; Cullen, WG; Williams, ED; Hunyadi, SE; Murphy, CJ (2007) Surface Morphology and Step Fluctuations on Silver Nanowires, **Surface Science**, 601: 4939- 4943.

10. Hunyadi Murph SE, Larsen G, Lascola, R (2016) Multifunctional Hybrid Fe2O3-Au Nanoparticles for Efficient Plasmonic Heating**. J. Visual Experiments (JOVE)** 108: e53598.

11. Hunyadi Murph SE, Lawrence K, Sessions H, Brown M, Larsen G (2020) Controlled Release of Hydrogen Isotopes from Hydride-Magnetic Nanomaterials, **ACS Applied Materials & Interfaces**, 12:9478-9488.

12. Hunyadi Murph SE, Jacobs S, Siegfried M, Hu T, Serkiz S, Hudson J. (2012) Manganese-Doped Gold Nanoparticles as Positive Contrast Agents for Magnetic Resonance Imaging (MRI) **J. Nanoparticle Res.**, 14: 658-659.

13. Hunyadi Murph SE, Sessions H, Lawrence K, Brown M, Ward, P (2021) Efficient Thermal Processes using Alternating Electromagnetic Field for Methodical and Selective Release of Hydrogen Isotopes, **Energy and Fuels**, 35: 3438-3448.

14. Li D, Seaman J, Hunyadi Murph SE, Kaplan D, Taylor-Pashow T (2019) Porous iron material for TcO_4^- and ReO_4^- sequestration from groundwater under ambient oxic conditions. **Journal of Hazardous Materials**, 374:177-185.

15. Pelaez, M. et al, (2012) A Review on the Visible Light Active Titanium Dioxide Photocatalysts for Environmental Applications, **Applied Catalysis B: Environmental**, 125: 331– 349.

16. Li L, Yan J, Wang T, Zhao ZJ, Gong J, Guan N, (2015) Sub-10 nm rutile titanium dioxide nanoparticles for efficient visible-light-driven photocatalytic hydrogen production, **Nature Comm.**, 6: 5881.

17. Wang X, Caruso R., (2010) Enhancing photocatalytic activity of titania materials by using porous structures and the addition of gold nanoparticles, **J. Mater. Chem.** 21: 20-28.

18. Chaudhuri RG, Paria S (2011) Core/Shell Nanoparticles: Classes, Properties, Synthesis Mechanisms, Characterization, and Applications, **Chemical Reviews**, 112: 2373-433.

19. Cappelletti, AL et al, (2015) Synthesis, Characterization, and Nanocatalysis Application of Core–Shell Superparamagnetic Nanoparticles of Fe3O4@Pd, **Australian J. of Chem.** 68:1492-1501.

20. Larsen, G, Farr, W, Hunyadi Murph, SE (2016) Multifunctional Fe2O3-Au Nanoparticles with Different Shapes: Enhanced Catalysis, Photothermal Effects, and Magnetic Recyclability, **J. Phys. Chem. C**, 120: 15162- 15172.

21. Hunyadi Murph, SE.; Serkiz, S.; Fox, E.; Colon-Mercado, H.; Sexton, L.; Siegfried, M. (2011) Synthesis, Functionalization, Characterization and Application of Controlled Shape

Nanoparticles in Energy Production, Fluorine-Related Nanoscience with Energy Applications, ACS Symposium Series, Volume 1064, Chapter 8, 127-163.

22. Hunyadi, SE, Murphy, CJ (2006) Tunable One-Dimensional Silver-Silica Nanopeapod Architectures, **J. Phys. Chem. B**, 110: 7226 -7231.

23. Yoon, Cm, Jang Y, Lee S, Jang J (2018) Dual electric and magnetic responsivity of multilayered magnetite-embedded core/shell silica/titania nanoparticles with outermost silica shell, **J. Mater. Chem. C**, 6:10241.

24. Misra, NN (2015) The contribution of non-thermal and advanced oxidation technologies towards dissipation of pesticide residues, **Trends in Food Science & Technology**, 45: 229–244.

25. He, Y, Basnet, P, Hunyadi Murph, SE, Zhao, Y (2013) Ag Nanoparticle Embedded TiO2 Composite Nanorod Arrays Fabricated by Oblique Angle Deposition: Toward Plasmonic Photocatalysis, **ACS Applied Materials & Interfaces**, 5: 11818-11827.

26. Hunyadi Murph, SE (2011), One-Dimensional Plasmonic Nano-photocatalysts: Synthesis, Characterization and Photocatalytic Activity, Solar Hydrogen and Nanotechnology VI, edited by Yasuhiro Tachibana, Proc. of SPIE, 81090T: 1-11.

27. Kun, Y, Basnet, P, Sessions, H, Larsen, G.; Hunyadi Murph, SE, Zhao, Y (2016) Fe2O3/TiO2 Core-Shell Nanorod Array for Visible Light Photocatalysis" **Catalysis Today**, special issue C1 Catalytic Chemistry, 51-58.

28. Hunyadi Murph, SE, Sessions, H, Kun, Y, Zhao, Y (2014) Nanocomposite Photocatalysts: Conversion of CO2 to Fuel, "**C1 Chemistry**", Division of Energy and Fuels (ENFL) at 249th American Chemical Society (ACS) National Meeting.